Experimental Investigation of Coupled Hydro-mechanical Behavior of Geopolymer Interfaces

Xingxing Qi, Nicolas Gay, Jean-philippe Carlier, Yun Jia, Matthieu Briffaut
Univ. Lille, CNRS, Centrale Lille, UMR 9013 - LaMcube - Laboratoire de Mécanique, Multiphysique, Multi-échelle, F-59000 Lille, France
Corresponding author: Xingxing Qi (e-mail: xingxing.qi@centralelille.fr)

ABSTRACT The importance of green repair materials lies in their ability to provide sustainable solutions for infrastructure maintenance while minimizing environmental impact through reduced resource consumption and lower emissions. This study explores the application of geopolymer, a sustainable and eco-friendly material, as a promising option. Specifically, this research focuses on the potential of metakaolin-based geopolymer. The fundamental mechanical properties and feasibility of geopolymer mortar were investigated through flexural strength, compressive strength, and uniaxial compression tests. Additionally, experiments designed following Darcy's Law were conducted to comprehend the permeability characteristics. These experiments revealed a significant water saturation influence on permeability, which decreases with increasing air pressure and confining pressure. Then, the porosity of this geopolymer mortar is 26.87% using gas while 18.54% using water. Further, a series of shear bond tests were performed to explore the hydro-mechanical behavior at the interface between geopolymer mortar and Ordinary Portland Concrete (OPC) under loading conditions. The results indicate commendable bonding performance at the interface, exhibiting a bond strength of $6.00\,\mathrm{MPa}$, signifying the potential for further research and application.
Keywords Geopolymer; Interfaces; Hydro-mechanical behavior; Shear strength; Repair materials

I. INTRODUCTION

A significant portion of national infrastructure was constructed approximately fifty years ago and now requires substantial repair and maintenance. Environmentally sustainable repair materials with a reduced carbon footprint have been in great demand by the construction industry worldwide. The concept of geopolymers was initially introduced as a new material by Davidovits (1991). Huseien et al. (2017) investigated cement-free geopolymer mortars, prepared from waste materials with a high content of silicate and aluminum and activated by alkaline solutions. These mortars are emerging as prominent sustainable repair materials. Zhang et al. (2014) explored that geopolymer binders are preferred because they generate 70–80% less carbon dioxide and have remarkably lower greenhouse gas emissions than ordinary Portland cement. McLellan et al. (2011), Duxson et al. (2007) showed that these new binders are highly sought after due to their enhanced durability, sustainability, and environmental friendliness.

Numerous scholars have attempted to utilize geopolymer mortar as a repair material for concrete. Momayez et al. (2005) found that the bond strength between the substrate concrete and the repair material

TABLE 1. Chemical Composition of Metakaolin Powder (by weight)

Metakaolin	SiO_2	Al_2O_3	Fe_2O_3	TiO_2	K_2O	CaO	MgO	SO_3	ZrO_2	Fire loss
Argicem (%)	60.53	29.64	4.68	1.72	0.65	1.41	0.95	0	0.15	0.27

played a decisive role when selecting geopolymers as repair materials. Mirza et al. (2014) studied the bond strength between mortar substrate and geopolymer in sandwich specimens. Geopolymer exhibited higher bonding strength than that of a comparable OPC mixture. Suksiripattanapong et al. (2015), Songpiriyakij et al. (2011) attempted to utilize geopolymer as a repair material by testing their slant shear, pull-out, and direct shear tests. Laskar & Talukdar (2017) found that ultra-fine slag based geopolymer had promising bond strength with rebar and old concrete.

Several methods have been developed to test shear strength. Common among these is the slant shear test, which achieves its objective by creating an angled interface. However, the shear behavior is influenced by the applied loading stress. Phoo-ngernkham et al. (2015) used slant test to investigate bond strength high calcium fly ash geopolymer mortars (GPM) containing OPC. Additional commonly used methods include the push-off test and the Z-method. These experimental designs feature loads applied perpendicular to the interface, more closely approximating real-world conditions. The sandwich test as mentioned above used push-off test, developed by Mirza et al. (2014). Purwanto et al. (2022) explored the shear-bond characteristics between self-compacting geopolymer concrete and conventional concrete using Z method. The direct bi-surface test and the one-plane shear method are designed to create a perpendicular interface between two parts. Shear is achieved by applying opposing shear forces to the two sections or by fixing one part while applying force to the other. This testing approach is conceptually straightforward, yet it places high demands on the experimental apparatus, requiring specially designed rigid loading plates to ensure uniform stress distribution. Alanazi et al. (2016) employed a compression-shear test that used a pressure pump to apply shear loads horizontally. In this research, the one-plane shear method was employed with an ingeniously designed semi-cylindrical steel loader to ensure even stress distribution. Additionally, a servo-controlled confining pressure system was used to prevent any eccentricity of the specimen.

The objective of this study was to explore the feasibility of geopolymer mortar by investigating its key characteristics. Further research focused on the bond performance between geopolymer and OPC. Additionally, the study simultaneously monitored changes in permeability during the loading process.

II. Materials and methods

A. Geopolymer mortar and substrate

In this research, geopolymer mortar was prepared using alkali-activated technology. The process flow diagram for its production is presented in Figure 1. The geopolymer was produced by blending, curing, and maintaining the precursor materials, standard sand, and a pre-prepared alkali-activating solution. The precursor employed was metakaolin powder, commercially known as Argicem, a form of metakaolin developed by Argeco Développement. This was produced through the flash calcination of kaolin clay. The results of the chemical composition tests are presented in Table 1.

The alkaline-activated solution was prepared using Betol K 5020 T, flake potassium hydroxide (KOH), and laboratory-grade water. The preparation process involved stirring for 30 minutes, followed by a 24-hour settling period. During the stirring process, a significant amount of heat was generated. To ensure the consistent quality of the solution, the mixed solution was sealed. The chemical composition of Betol K 5020

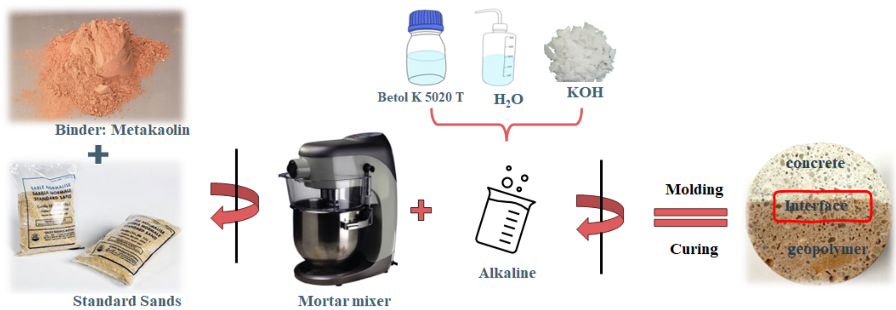

FIGURE 1. Geopolymer Mortar Preparation Flowchart

TABLE 2. Chemical Composition of Betol K 5020 T (by mass)

Product	SiO_2	Na2O	K_2O	Molar Ratio
Betol K 5020 T(%)	30	0	18.5	2.54

T is shown in Table 2.

B. Mix proportion and specimen design

Mixing was performed using a professional standard method. Initially, the solid mixture was mixed in the mixer pot at a slow speed for 30 seconds. Subsequently, the alkali-activated solution was added and stirred slowly for 60 seconds, followed by a fast stir for 30 seconds. After a pause of 90 seconds, the mixture was given a final rapid stir for 60 seconds. Once the specimen was cast, it was placed in a curing box with conditions of $20.8\,°C$ temperature and 90% relative humidity (RH).

In this study, the composition of the geopolymer paste used is based on mass percentages, with BETOL 5020T constituting 39%, potassium hydroxide (KOH) 7%, and laboratory-grade water 6%. Additionally, the SiO_2/K_2O ratio was 3.40. The precursor utilized was metakaolin, constituting 48% of the mixture. As for the mortar, standard sand accounts for 65.31% based on total paste mass. All the studies in this research were conducted at the mortar level.

The setting time of the geopolymer mortar was tested in accordance with EN 196-3. The test results indicated that the initial setting time of the geopolymer mortar is 420 minutes, while the final setting time is 600 minutes.

C. Experimental device and methods

2.3.1 Machanical strength on geopolymer mortar

Flexural strength and compressive strength test. To assess the mechanical properties of geopolymer mortar, specimens with dimensions of $40mm \times 40mm \times 160mm$ were prepared and subjected to a curing process for 14 days. The flexural strength test was conducted initially using an Instron testing machine, in compliance with the standards set forth in EN 12390-5. The flexural strength is calculated according to Equation 1.

$$\sigma_f = \frac{3FL}{2bd^2} \tag{1}$$

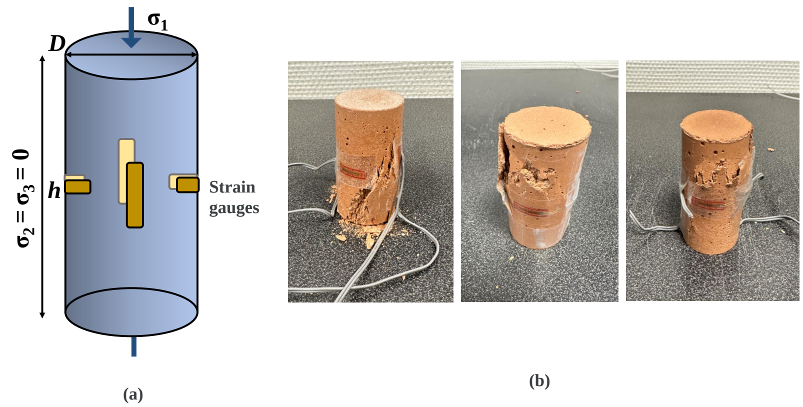

FIGURE 2. **Uniaxial Compression Test(a) and Damaged Specimens Following Tests(b)**

Here, σ_f represents the flexural strength, F is the load at the fracture point, L is the length of the support span, b is the width of the specimen, and d is the depth of the specimen.

Upon failure, the fractured specimens were then tested for compressive strength under EN 12390-3. which is obtained by dividing the fracture point force by the area subjected to the force.

Uniaxial compression test on geopolymer mortar. In this study, uniaxial compression tests were performed using an Instron testing machine, as shown in Figure 2, to assess the mechanical properties of both geopolymer mortar and Ordinary Portland Cement (OPC) specimens. The tests focused on measuring compressive strength, elastic modulus, and Poisson's ratio. Each specimen had a diameter of 37 mm and a height of 74 mm. The geopolymer mortar samples were cast and cured for 14 days. OPC specimens of identical dimensions were prepared by extracting cores through drilling for comparative analysis. During testing, the strain was monitored with four strain gauges on each specimen, two aligned horizontally and two vertically.

2.3.2 Permeability and porosity

Permeability Test. The gas permeability test is a method used to determine the resistance of materials such as concrete, rocks, or films to gas flow, based on the principles of Darcy's Law, which governs the flow of fluids through porous media. The experimental setup and its underlying principles are detailed Figure 3. For this test, cylindrical specimens measuring $36\,\mathrm{mm}$ in both diameter and height were utilized. The procedure involves recording the upstream pressure P_1 and downstream pressure P_0 under conditions that approach steady-state, ensuring constant flow. The distribution of pressure during the test is governed by the relationship outlined in Equation 2, the variable x is used to describe how the pressure varies at different points within the specimen when a constant volumetric flow rate is maintained. This setup allows for precise measurements of gas permeability, providing critical insights into the material's porosity and structural integrity.

$$\nabla^2 P^2 = 0 \quad and \quad P(x) = \sqrt{P_1^2\left(1 - \frac{x}{L}\right) + P_0^2\frac{x}{L}} \tag{2}$$

In the formula, Q_1 and Q_0 denote the volumetric flow rates of gas on the upstream and downstream sides of the sample, respectively; L represents the height of the specimen, and x represents the position along the length of the specimen in the direction of gas flow.

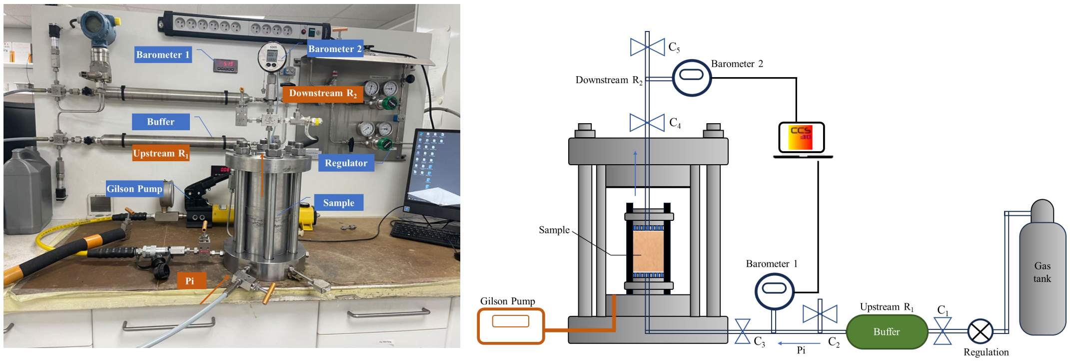

(a) Photograph of the permeability apparatus **(b) Schematic diagram of the permeability apparatus**

FIGURE 3. Permeability Testing Apparatus

$$Q_1 = \frac{KA}{2\mu L}\left(\frac{P_1^2 - P_0^2}{P_1}\right) \tag{3}$$

$$Q_0 = \frac{KA}{2\mu L}\left(\frac{P_1^2 - P_0^2}{P_0}\right) \tag{4}$$

In the equation, K denotes the specimen's permeability, A represents the cross-sectional area for fluid flow. Given that μ, the dynamic viscosity, was 2.2×10^{-5} in this study. To determine the permeability K, one must accurately measure the volumetric flow rates Q_1 and Q_0.

Initially, gas was injected at a constant pressure P_i. Once a constant flow was established, valve C_1 was closed, and the upstream reservoir R_1 began supplying the sample with gas. The first measurement aimed to determine the incoming flow rate Q_1, which corresponds to the average flow rate Q_1^{moy} over a time interval Δt. During this interval, a pressure drop ΔP_1 occurred in R_1. Assuming that the flow rate remains constant during Δt and calculating the average injection pressure as $P_1^{moy} = P_1 - \Delta P_1/2$, the flow rate Q_1 was then accurately deduced in Equation 5.

$$Q_1^{moy} = \frac{V_1 \Delta P_1}{P_1^{moy} \Delta t} \tag{5}$$

V_1 is the volume of reservoir R_1, which also includes the volume of the tubing between R_1 and the sample. This combined volume is established through precise calibration.

The permeability K can be calculated using Equation 3, where P_1 is the average pressure P_1^{moy}, and Q_1 is the average flow rate Q_1^{moy}. This approach, known as the quasi-constant flow rate method, is employed at high pressures on the upstream side of the sample. The initial procedure for the downstream quasi-steady method mirrors the steps previously described. After establishing a presumed steady flow (refer to Figure 3), valve C_5 is closed, leading to an increase ΔP_0 in the atmospheric pressure P_0 due to the gas flow. This change demonstrates that:

$$Q_0^{moy} = \frac{V_2 \Delta P_0}{P_0^{moy} \Delta t} \tag{6}$$

V_2 represents the volume of the reservoir R_2, which includes the tubing connecting the sample to R_2. The average P_0 is calculated as $P_0^{moy} = P_0 + \Delta P_0/2$. In this experiment, the volume V_2 is measured to be $6.349\,\mathrm{mL}$. Finally, based on the established relationships, the permeability can be expressed as shown in Equation 7.

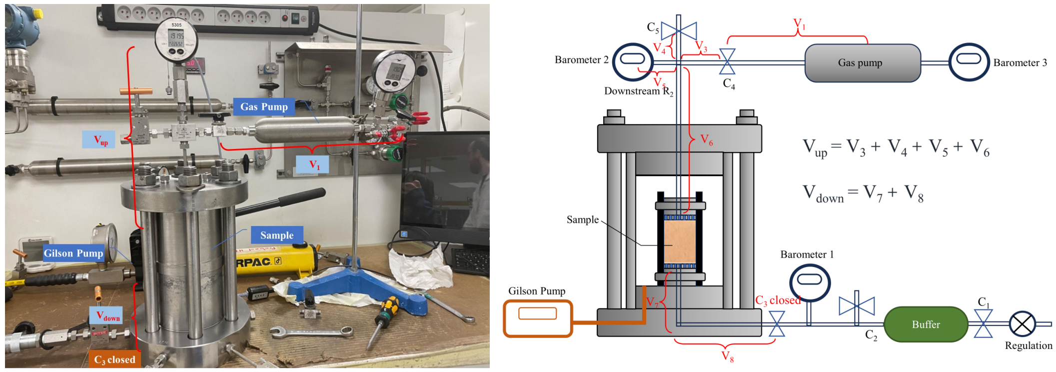

(a) Photograph of the porosity apparatus (b) Schematic diagram of the porosity apparatus

FIGURE 4. Porosity Testing Apparatus

(a) Smooth surface of concrete cylinder (b) Specimens' preparation (c) Specimens to be sheared after grinding

FIGURE 5. Interface and Specimens' Preparation

$$K = \frac{\mu \cdot Q_0^{moy} \cdot 2 \cdot L \cdot P_0^{moy}}{A \cdot ((P_0^{moy})^2 - P_0^2)} \tag{7}$$

Porosity Test. The porosity was measured by initially determining the volume of the specimen using Boyle's Law, which states that the pressure and volume of a given amount of gas are inversely proportional at constant temperature. The permeability testing apparatus was modified by integrating a gas pump with a known volume V_1 and an initial pressure P_1. The system was then connected, and the pressure was stabilized at P_2, as depicted in Figure 4. Using Boyle's Law, the unknown volume V_{sample} was calculated from the relationship $P_1V_1 = P_2V_2$. It was determined that $V_{sample} = V_2 - V_1 - V_{up} - V_{down}$, where V_{up} refers to the volume of the upstream piping system and V_{down} to the volume of the downstream system. Porosity was then calculated by comparing the geometric volume of the specimen to its actual volume.

Additionally, the vacuum drainage method is employed to test the porosity of specimens, providing a comparison to the results obtained from the gas tests.

2.3.3 Hydro-mechanical behaviour under shear loading

Specimen Preparation. In this project, the interface between geopolymer mortar and concrete was studied, as depicted in Figure 5. The semi-cylindrical concrete specimens used had a diameter of 65 mm and a height of 60 mm. Both ends of each specimen were polished to achieve a flat and smooth finish, ensuring uniform stress distribution during testing.

The semi-cylindrical concrete specimens were positioned in cylindrical molds with a diameter of 65 mm and a height of 60 mm. The mixed geopolymer mortar was then poured into the remaining half of the

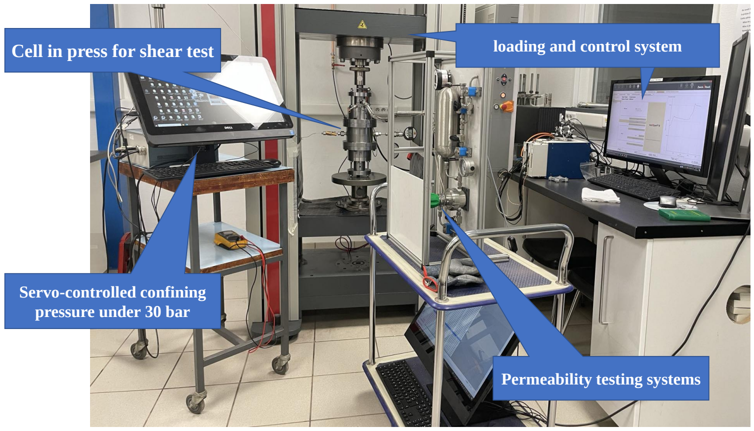

FIGURE 6. Photograph of the Shear Test Apparatus

cylindrical molds. These specimens were cured until no further mass change was observed, typically over a period of 14 days. Excess material at both ends of the specimens was carefully ground down to create a flat and smooth surface, which is essential for facilitating the subsequent shear testing.

Shear Test Apparatus. The entire experimental setup comprises four modules, as shown in Figure 6. The first module is the loading and control system, which includes a materials testing machine, TestControl II machine electronics, and TestXpert III testing software. This system provides physical support for the shearing process and control over the loading speed. High-resolution acquisition of each travel and force peak is synchronously recorded across all measuring channels. The experiment employs displacement control at a speed of $0.12\,\mathrm{mm/min}$.

The second module is the cell in press for the shear test, as illustrated in Figure 7. The internal structure of this module is shown in the accompanying diagram. It facilitates the transmission of the load and ensures the correct application of interface shear loading. An initial confining pressure of $30\,\mathrm{bar}$ is established within the cell. The shear force applied at the interface is generated by converting an axial force, which is skewed at the interface, with the aid of a designed system. Inside the cell, a rubber sleeve connects to the confining pressure space, creating a confining pressure that acts perpendicular to the axial force on the interior specimen. Considering that the strength of concrete exceeds that of geopolymer mortar, concrete is used as the force-bearing side. A soft foam pad is included to accommodate displacement differences during shearing. The shear stress is exclusively generated by the axial deviatoric stress loading.

The third module is a servo-controlled confining pressure system, maintained at a fixed confining pressure using the MiniPompe system. This dynamically balanced device ensures that the confining pressure is consistently regulated at $30\,\mathrm{bar}$, accommodating variations that may occur during specimen assembly and loading.

The fourth module is the permeability testing system, designed to measure and record the permeability values K and the volumetric flow rate Q at different stages of the shearing load process. In this study, Darcy's law was used to calculate the permeability values under dynamic loading conditions. Permeability tests were conducted at intervals of every $0.2\,\mathrm{mm}$ of loading displacement. Since the interface acted as a point of weakness, permeability was considered to occur exclusively at this location. The evaluation of permeability was divided into two phases: before specimen failure, permeability was calculated based on

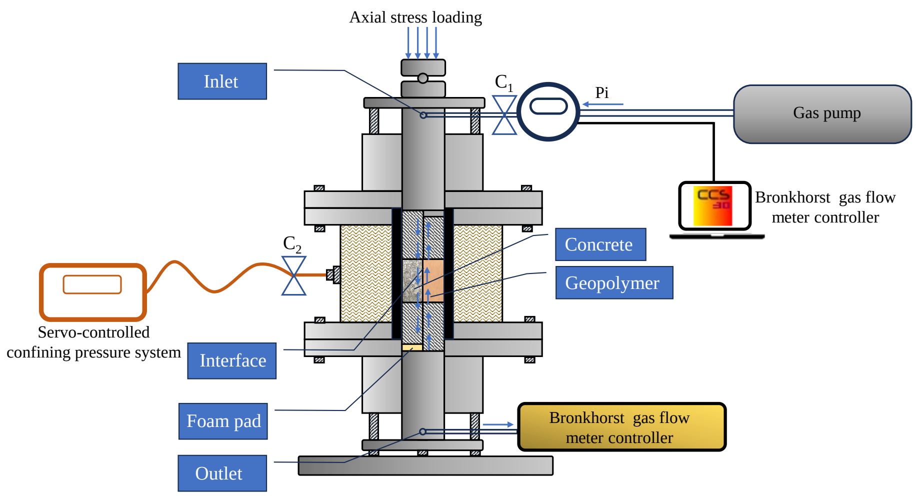

FIGURE 7. **Schematic Diagram Cell in Press for Shear Test**

the change in air pressure at the inlet over a fixed duration; after failure, due to rapid changes in air pressure, recording pressure changes over a set time became challenging. Consequently, the flow rate of gas at the outlet was measured using a Bronkhorst gas flow meter controller. The permeability K was calculated using a modified form of Darcy's law for gas flow through the interface. For the pre-failure phase, ΔP was achieved by recording the time required to achieve a fixed pressure change at the incoming side. For the post-failure phase, Q was measured directly using the flow meter. According to Equations 5 and 6, the permeability value can be similarly calculated. This approach facilitated the determination of permeability during both stable and rapid phases of the loading process, highlighting the weak interface's influence on the overall specimen behavior.

Shear Stress Calculation. The shear stress, represented by σ, is calculated as the ratio of the maximum force F_{max} to the area of the interface A_{int}. Mathematically, it is expressed as:

$$\sigma = \frac{F_{\max}}{A_{int}} \tag{8}$$

where σ represents the shear stress, F_{max} is the maximum force applied, and A_{int} is the area of the interface. The shear strength refers to the stress at the point of maximum force during the shearing process.

III. Results and discussion

A. Machanical strength on geopolymer mortar

3.1.1 Flexural strength and compressive strength test

Three specimens measuring 160 mm in length, 40 mmin width, and 40 mm in depth were prepared for testing their flexural strengths. The results of the flexural strength tests yielded values of approximately 7.83 MPa, 8.57 MPa, and 7.17 MPa, respectively. The average flexural strength of the three specimens is approximately 7.86 MPa. While the flexural strength might appear lower compared to traditional Portland cement-based mortars, it is generally adequate for many construction and repair applications where extreme bending forces are not the dominant stress factor.

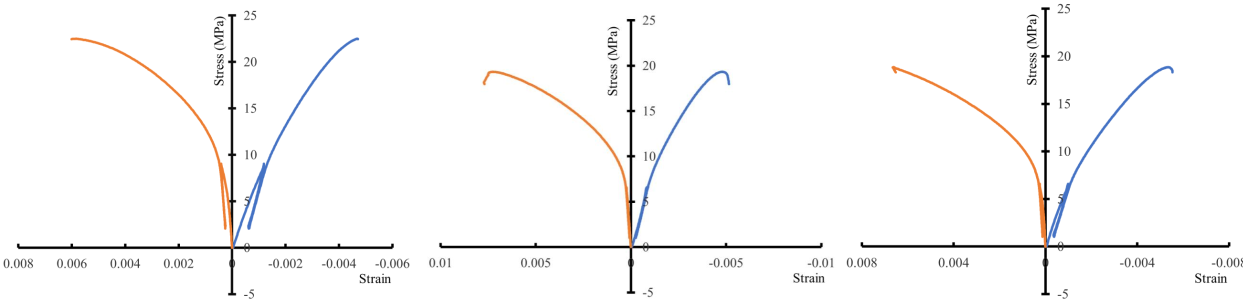

(a) GM-1 **(b) GM-2** **(c) GM-3**

FIGURE 8. Uniaxial Compression Stress-strain Curve for Geopolymer Mortar Sample

TABLE 3. Elastic Modulus and Poisson's ratio

	MG-1	MG-2	MG-3	Average
E(GPa)	11.59	9.27	8.53	9.80
ν	0.28	0.27	0.21	0.25

After conducting the flexural strength tests, the six fractured specimens were used for compressive strength testing. The compressive strengths recorded were as follows: $39.12\,\mathrm{MPa}$, $39.39\,\mathrm{MPa}$, $40.78\,\mathrm{MPa}$, $41.68\,\mathrm{MPa}$, $39.99\,\mathrm{MPa}$, and $42.27\,\mathrm{MPa}$. Compared to traditional concrete, a average compressive strength of $40.54\,\mathrm{MPa}$ indicates that this geopolymer mortar is competitive in terms of load-bearing capacity. This strength is sufficient to meet the structural demands of residential and commercial buildings, especially in applications such as non-load-bearing walls, floors, and overlays.

3.1.2 Uniaxial compressive test

Figure 8 illustrates the uniaxial compression stress-strain curves for three geopolymer mortar specimens, labeled MG-1, MG-2, and MG-3, which were prepared with identical mix proportions and subjected to the same curing conditions. The experimental results depicted by the curves represent the mechanical response of the geopolymer mortar when subjected to compressive loads. The red curves on the left side of each graph represent the circumferential stress-strain response, which is typically associated with the lateral deformation of the specimens under compression. The blue curves on the right side illustrate the axial stress-strain response under the applied load, correlating with the longitudinal deformation.

The data points where the stress peaks correspond to the compressive strength of the specimens. From the initial linear portion of the axial stress-strain curves (blue), the elastic modulus, indicative of the material's stiffness, can be determined. It is derived from the slope of this linear region. The Poisson's ratio, which quantifies the ratio of lateral strain to axial strain, can be deduced from the lateral and axial deformation measurements. The results of the elastic modulus and Poisson's ratio of the geopolymer mortar are presented in Table 3.The average elastic modulus is $9.80\,\mathrm{GPa}$. A lower modulus of elasticity implies greater deformation under stress, potentially beneficial for applications requiring some flexibility. The average Poisson's ratio is 0.25, comparable to many conventional construction materials.

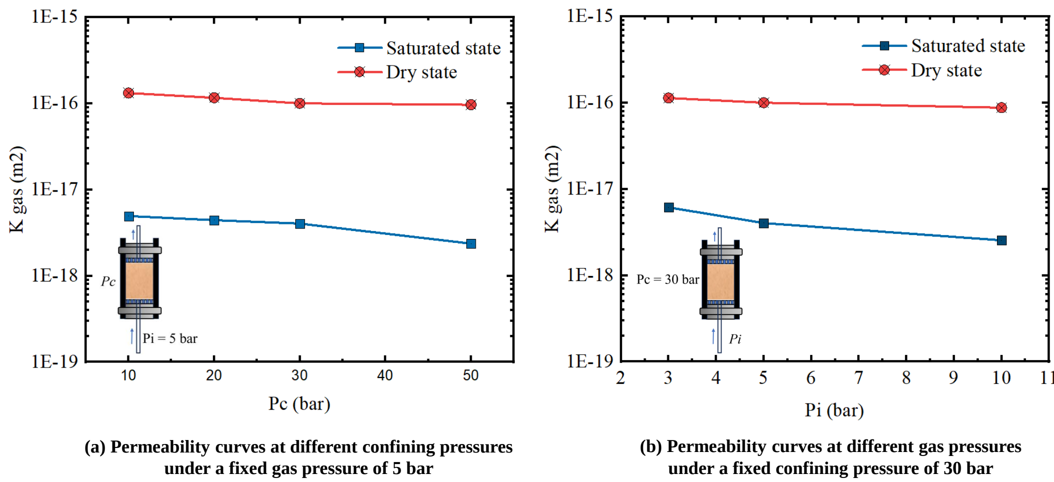

FIGURE 9. Permeability Curves Under Varying Pressures

B. Permeability and porosity

3.2.1 Permeability

Figure 9 demonstrates the permeability trend of geopolymer mortar, with permeability value K varying under different conditions. For the material in its saturated state, the permeability is approximately $4 \times 10^{-18}\,\mathrm{m}^2$. whereas, in the dry state, the permeability is about $1 \times 10^{-16}\,\mathrm{m}^2$.

The curves in Figure 9 (a) show the permeability response to varying confining pressures P_c at a fixed inlet gas pressure of $5\,\mathrm{bar}$. It can be observed that an increase in confining pressure results in a decrease in permeability for both states. This suggests that the geopolymer mortar's pore structure becomes more compressed under higher confining pressures, thus reducing the flow pathways for the gas. Figure 9 (b) presents the permeability behavior under different inlet gas pressures P_i at a constant confining pressure of $30\,\mathrm{bar}$. The observed decrease in permeability of geopolymer mortar under both saturated and dry conditions with increasing gas pressure can be primarily attributed to pore compression. In the saturated state, higher gas pressure could force water to block more of the pore pathways, thereby reducing the permeability. In the dry state, the pressure might cause a compaction of the pore structure, again leading to decreased permeability.

3.2.2 Porosity

Utilizing Boyle's Law through a gas test method represents the relationship between pressure and volume, the porosity was determined to be 26.87%. Conversely, the vacuum saturation method yielded a lower porosity value of 18.54%. The discrepancy between the two porosity measurements could be attributed to the intrinsic differences in the methods' sensitivity to the types of pores detected. The gas test method might register both open and closed pores, whereas the vacuum saturation method is more likely to measure only those pores accessible to fluids under pressure. This phenomenon is in line with expectations.

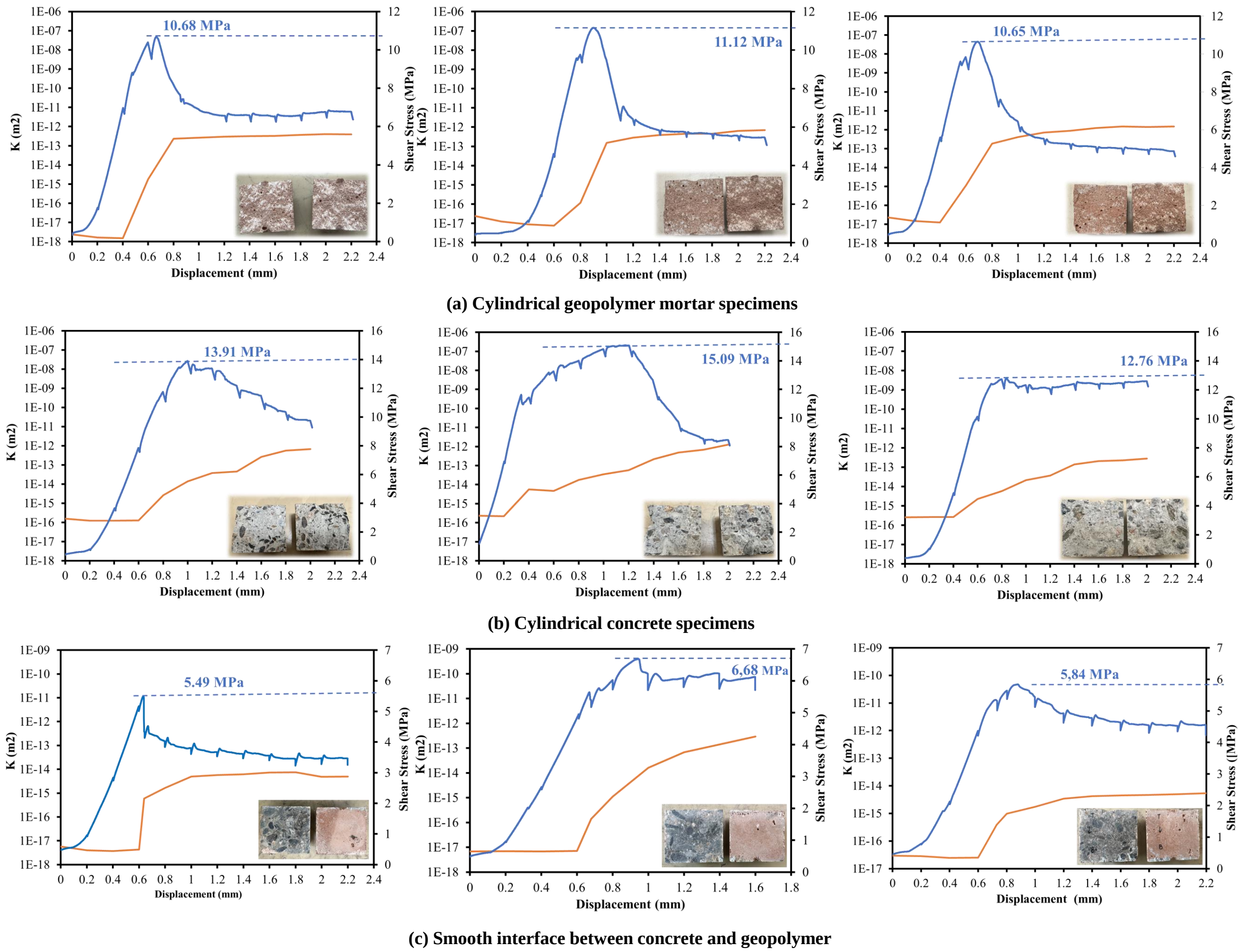

(a) Cylindrical geopolymer mortar specimens

(b) Cylindrical concrete specimens

(c) Smooth interface between concrete and geopolymer

FIGURE 10. **Stress and Permeability Curves Under Shear Loading for Interfaces with Varying Materials**

C. *Shear bond strength between geopolymer and OPC*

Figures 10 presents stress and permeability curves under shear loading for interfaces with varying materials under the servo-controlled confining pressure of $30\,\mathrm{bar}$. In the depicted shear tests, three specimens were prepared for each experimental condition to ensure reliability and reproducibility of results. The blue curves represent the evolution of shear strength during the loading process, while the red curves indicate the changes in permeability, denoted as K, over the course of loading.

IV. Conclusions

This study investigates the potential of geopolymers as a repair material, examining their mechanical strength, permeability, and porosity as critical factors influencing the performance of geopolymer mortars. Through meticulously designed experiments, the bond strength between the geopolymer and Ordinary Portland Cement (OPC) was scrutinized, concurrently observing variations in permeability. The main conclusion are as follows.

The geopolymer mortar under examination demonstrates an average flexural strength of $7.86\,\mathrm{MPa}$ and an average compressive strength of $40.54\,\mathrm{MPa}$. The reported average elastic modulus of the material is

$9.80\,\mathrm{GPa}$, with an average Poisson's ratio of 0.25. These mechanical properties suggest that the geopolymer mortar offers a commendable balance of flexibility and rigidity, making it a suitable candidate for repair applications. The elastic modulus and Poisson's ratio further reveal the material's ability to deform elastically under stress, which is a desirable trait for materials used in restoration, as it can accommodate movements and loading conditions.

The permeability K of geopolymer mortar in its saturated state was found to be approximately $4 \times 10^{-18}\,m^2$, while in a dry state it was approximately $1 \times 10^{-16}\,m^2$. The study observes that an increase in both confining pressure and inlet gas pressure leads to a reduction in the material's permeability. The porosity measurements obtained through Boyle's Law and the vacuum saturation method showed considerable variation, with the former method indicating a porosity of 26.87 % and the latter 18.54 %.

The interface between geopolymer and OPC, when smooth and subjected to a servo-controlled confining pressure of 30 bar, demonstrates an average shear strength of $6.00\,\mathrm{MPa}$. This substantial bond strength highlights the potential of geopolymer as a promising repair material. The shear strength curve is categorized into three distinct phases: the Ascending Phase, the Descending Phase, and the Stable Phase. Throughout these stages, permeability was meticulously monitored, exhibiting a trend that initially shows a slight decline, followed by an increase, and ultimately stabilizing. This pattern of permeability changes aligns with the structural adjustments within the material under varying stress levels, underscoring the dynamic interaction between mechanical strength and fluid transmission capability.

Looking ahead, quantification of interface roughness and simulation studies will be vital to further understand and predict the mechanical interlocking and fluid flow behaviors observed. Additionally, microscopic research at the interface is more conducive to discovering the essence.

References

Alanazi, H., Yang, M., Zhang, D. & Gao, Z. J. (2016), 'Bond strength of PCC pavement repairs using metakaolin-based geopolymer mortar', *Cement and Concrete Composites* **65**, 75–82.

Davidovits, J. (1991), 'Geopolymers: inorganic polymeric new materials', *Journal of Thermal Analysis and calorimetry* **37**(8), 1633–1656.

Duxson, P., Provis, J. L., Lukey, G. C. & Van Deventer, J. S. (2007), 'The role of inorganic polymer technology in the development of 'green concrete'', *cement and concrete research* **37**(12), 1590–1597.

Huseien, G. F., Mirza, J., Ismail, M., Ghoshal, S. K. & Hussein, A. A. (2017), 'Geopolymer mortars as sustainable repair material: A comprehensive review', **80**, 54–74.
URL: *https://www.sciencedirect.com/science/article/pii/S1364032117307207*

Laskar, S. M. & Talukdar, S. (2017), 'Preparation and tests for workability, compressive and bond strength of ultra-fine slag based geopolymer as concrete repairing agent', **154**, 176–190.
URL: *https://www.sciencedirect.com/science/article/pii/S0950061817315301*

McLellan, B. C., Williams, R. P., Lay, J., Van Riessen, A. & Corder, G. D. (2011), 'Costs and carbon emissions for geopolymer pastes in comparison to ordinary portland cement', *Journal of cleaner production* **19**(9-10), 1080–1090.

Mirza, J., Durand, B., Bhutta, A. R. & Tahir, M. M. (2014), 'Preferred test methods to select suitable surface repair materials in severe climates', *Construction and Building Materials* **50**, 692–698.

Momayez, A., Ehsani, M., Ramezanianpour, A. & Rajaie, H. (2005), 'Comparison of methods for evaluating bond strength between concrete substrate and repair materials', *Cement and concrete research* **35**(4), 748–757.

Phoo-ngernkham, T., Sata, V., Hanjitsuwan, S., Ridtirud, C., Hatanaka, S. & Chindaprasirt, P. (2015), 'High calcium fly ash geopolymer mortar containing Portland cement for use as repair material', *Construction and Building Materials* **98**, 482–488.

Purwanto, Ekaputri, J. J., Nuroji, Indriyantho, B. R., Han, A. & Gan, B. S. (2022), 'Shear-bond behavior of self-compacting geopolymer concrete to conventional concrete', *Construction and Building Materials* **321**, 126167.

Songpiriyakij, S., Pulngern, T., Pungpremtrakul, P. & Jaturapitakkul, C. (2011), 'Anchorage of steel bars in concrete by geopolymer paste', *Materials & Design* **32**(5), 3021–3028.

Suksiripattanapong, C., Horpibulsuk, S., Chanprasert, P., Sukmak, P. & Arulrajah, A. (2015), 'Compressive strength development in fly ash geopolymer masonry units manufactured from water treatment sludge', *Construction and Building Materials* **82**, 20–30.

Zhang, Z., Provis, J. L., Reid, A. & Wang, H. (2014), 'Geopolymer foam concrete: An emerging material for sustainable construction', *Construction and Building Materials* **56**, 113–127.